A kinome-wide synthetic lethal CRISPR/Cas9 screen reveals that mTOR inhibition prevents adaptive resistance to CDK4/CDK6 blockade in HNSCC

Yusuke Goto[1#], Keiichi Koshizuka[1#], Toshinori Ando[1,2], Hiroki Izumi[1], Xingyu Wu[1], Kuniaki Sato[1], Tomohiko Ishikawa[1], Kyle Ford[3], Xiaodong Feng[1], Zhiyong Wang[1], Nadia Arang[1], Michael M. Allevato[1], Ayush Kishore[1], Prashant Mali[3], J. Silvio Gutkind[1*]

[1]Moores Cancer Center, University of California San Diego, La Jolla, CA 92093, USA

[2]Graduate School of Biomedical & Health Sciences, Hiroshima University, Japan

[3]Department of Bioengineering, University of California San Diego, San Diego, CA 92093, USA

#These authors contributed equally to this work

Running Title: mTOR and cell cycle inhibition in HNSCC

***Corresponding author:** J. Silvio Gutkind, Ph.D.

Professor, Department of Pharmacology

Associate Director of Basic Science, UC San Diego Moores Cancer Center

3855 Health Sciences Drive, #0803, room 2344, La Jolla, CA 92093

Tel: +1 (858) 534-5980

E-mail: sgutkind@ucsd.edu

Conflict of Interests

J.S.G. is consultant for Domain Therapeutics, Pangea Therapeutics, and io9, and founder of Kadima Pharmaceuticals, outside the submitted work.

Current affiliations:

YG: Department of Urology, Chiba University Graduate School of Medicine, Chiba, Japan

TA: Center of Oral Clinical Examination, Hiroshima University Hospital, Hiroshima, Japan

HI: Department of Thoracic Oncology, National Cancer Center Hospital East, Chiba, Japan

XF: State Key Laboratory of Oral Diseases, National Clinical Research Center for Oral Diseases, Research Unit of Oral Carcinogenesis and Management, Chinese Academy of Medical Sciences, Frontier Innovation Center for Dental Medicine Plus, West China Hospital of Stomatology, Sichuan University, Chengdu, Sichuan 610041, China

ZW: The Stomatology Hospital, Zhejiang University School of Medicine, Hangzhou, China

NA: Quantitative Biosciences Institute (QBI), University of California San Francisco, San Francisco, CA, 94158, USA

MA: Department of Otolaryngology-Head and Neck Surgery, University of Michigan Medical School, Ann Arbor, Michigan, USA

AK: Genentech inc.

Abstract

The comprehensive genomic analysis of the head and neck squamous cell carcinoma (HNSCC) oncogenome revealed the frequent loss of $p16^{INK4A}$ (*CDKN2A*) and amplification of cyclin D1 (*CCND1*) genes in most HPV negative HNSCC lesions. However, cyclin-dependent kinase 4 and 6 (CDK4/6) inhibitors have shown modest effects in the clinic. The aberrant activation of PI3K/mTOR pathway is highly prevalent in HNSCC, and recent clinical trials have shown promising clinical efficacy of mTOR inhibitors (mTORi) in the neoadjuvant and adjuvant settings but not in advanced HNSCC patients. By a kinome-wide CRISPR/Cas9 screen, we identified cell cycle inhibition as a synthetic lethal target for mTORi. Combination of mTORi and palbociclib, a CDK4/6 specific inhibitor, showed strong synergism in HNSCC-derived cells in vitro and in vivo. Remarkably, we found that adaptive increase in cyclin E1 (CCNE1) expression upon palbociclib treatment underlies the rapid acquired resistance to this CDK4/6 inhibitor. Mechanistically, mTORi inhibits the formation of eIF4G-*CCNE1* mRNA complexes, with the consequent reduction in mRNA translation and CCNE1 protein expression. Our findings suggest that mTORi reverts the adaptive resistance to palbociclib. This provides a multimodal therapeutic option for HNSCC by co-targeting mTOR and CDK4/6, which in turn may halt the emergence of palbociclib resistance.

Significance

A kinome-wide CRISPR/Cas9 screen identified cell cycle inhibition as a synthetic lethal target of mTOR inhibitor (mTORi). mTORi in combination with palbociclib, a CDK4/6 specific inhibitor, showed strong synergistic effects in head and neck squamous cell carcinoma. Mechanistically, mTORi inhibited palbociclib-induced increase in cyclin E1 (CCNE1).

Keywords: CRISPR screen, synthetic lethality, HNSCC, cell cycle, cyclin, mTOR inhibitor, palbociclib

Introduction

Head and neck squamous carcinoma (HNSCC) is among the ten most frequent cancers in the United States, with 54,540 new cases and 11,580 deaths estimated in the US alone in 2023 (1). Recent breakthrough treatment options by the use of immunotherapies targeting immune checkpoints brought survival benefit for HNSCC patients; however, the overall response rate to these immunotherapies in HNSCC is only ~20% (2). Thus, novel therapeutic options for this disease are urgently needed.

The comprehensive analysis of the HNSCC oncogenome revealed frequent loss of $p16^{INK4A}$ (*CDKN2A*) in HPV negative HNSCC, which account for 60% of the cases (3). Furthermore, amplification of the cyclin D1 (*CCND1*) gene is a frequent event in HNSCC, which has been reported to include 31% of the HPV negative HNSCC (3). However, cyclin-dependent kinase 4 and 6 (CDK4/6) inhibitors as single agents have shown modest effects regardless of *CDKN2A*-altered status in recurrent and metastatic HNSCC (4). Furthermore, a double-blind, randomized phase II trial (PALATINUS) that evaluated the efficacy of palbociclib plus cetuximab in patients with unselected HPV-unrelated recurrent or metastatic HNSCC did not significantly prolong the overall survival (OS) of patients with HNSCC (5). In this context, novel combinatory therapeutics for palbociclib based on molecular biological mechanisms is in needed. On the other hand, our group has been focusing on the study of mTOR signaling in HNSCC. Indeed, we have shown that the PI3K-mTOR pathway is the most frequently activated signaling mechanism in HNSCC, as judged by strong pS6 expression in more than 90% of HNSCC specimens (6). Based on these results, we have recently performed a clinical trial using rapamycin, which is a 1^{st} generation mTOR inhibitor (mTORi), in newly diagnosed HNSCC patients. Here, we found that rapamycin was effective for most of the HNSCC patients, with an overall response rate of 25 % including one case of complete response despite 21 days treatment duration (7). Similarly, we have recently shown that mTOR inhibition with everolimus diminish significantly the progression free survival of locally advanced HPV negative (HPV-) HNSCC lesions in the adjuvant setting (8). However, earlier clinical trials involving advanced, recurrent metastatic HNSCC patients showed limited response and resulted in treatment failure (9). The molecular mechanisms underlying mTORi resistance should be uncovered to find precise molecular targets which can be combined with mTORi to achieve durable responses.

In this study, we aimed to identify synthetic lethal targets and resistance mechanisms for mTORi by taking advantage of CRISPR/Cas9 screening. Using 2^{nd} generation mTORi, INK128, we identified cell cycle regulation pathway as one of most significant synthetic lethal targets and resistant pathways to mTORi in HNSCC. To explore the translational potential of these findings, we observed a strong synergism between INK128 and palbociclib, which is a widely used approved CDK4/6 inhibitor, *in vitro* and *in vivo*. In turn, we found that CCND1 and Cyclin E1 (CCNE1) accumulate upon palbociclib treatment, and that CCNE1 overexpression is sufficient to induce palbociclib resistance in HNSCC cells. Co-administration of INK128 and palbociclib could prevent the protein accumulation of CCNE1 by reducing its mRNA translation, and consequently, co-administration of these targeted agents can revert the resistance to palbociclib in CCNE1 overexpressing cells. Overall, our findings suggest that co-targeting mTOR and cell cycle signaling represents a potential therapeutic option for HNSCC. These findings may be also relevant for other cancer types characterized by the progressive acquisition of resistance to CDK4/6 inhibitors.

Materials and methods

Cell lines, culture conditions and chemicals. Human HNSCC cell lines Cal27 (RRID:CVCL_1107) and HN12 (RRID:CVCL_HN12) were genetically characterized as part of NIH/NIDCR Oral and Pharyngeal Cancer Branch cell collection given from NIH/NIDCR in 2016, and have been described previously (10). Only cell lines of <20 passages were used for experiments. All cell lines are frequently tested for mycoplasma contamination. No presence of mycoplasma was found according to MycoAlert (#LT07-418, Lonza, ME, USA). All cell lines were cultured in DMEM (D-6429, Sigma-Aldrich, St. Louis, MO), 10% fetal bovine serum (FBS) (F2442, Sigma-Aldrich), 1% antibiotic/ antimycotic solution (A5955, Sigma-Aldrich), 5% CO2, at 37°C. INK128 (I-3344) was purchased from LC Laboratories (Woburn, MA), and palbociclib (S1116) was purchased from Selleckchem (Houston, TX).

CRISPR screen. CRISPR screen was performed as previously described (11-13).

The two-vector system was used for this study. First, we generated Cas9-stably expressing Cal27 cells with lentiviral infection from lentiCas9-Blast. lentiCas9-Blast was a gift from Feng Zhang (Addgene plasmid # 52962; http://n2t.net/addgene:52962; RRID: Addgene_52962). The infected cells were selected with blasticidin (10 μg/mL) for 10 days. After confirming Cas9 expression by western blot, the Cal27-Cas9 cells were infected with two different gRNAs targeting AAVS locus, and were subjected to NGS to confirm cutting efficiency. The CRISPR cutting efficiency of Cas9 expressed cells was tested by two AAVS locus targeting sgRNA: gT1, and gT2 (Hygromycin B resistant). AAVS1 gene from genome DNA was amplified and then NEBnext primers (E7335S) were used to attach the sequencing adaptors. Sequencing data were analyzed using CRISPResso2 (http://crispresso.rocks/) (14). AAVS1 locus targeting sgRNA constructs (gT1/gT2) provided by Prashant's lab. Primer sequences for NGS (Next Generation Sequencing): NGS_AAVS1_F: ACACTCTTTCCCTACACGACGCTCTTCCGATCTTCCCAGGGCCGGTTAATGTGG; NGS_AAVS1_R: GACTGGAGTTCAGACGTGTGCTCTTCCGATCTTGCCTAACAGGAGGTGGGGGTTAG;

Amplicon reference sequence (+- 30bp around the PAM seq): TGCCTAACAGGAGGTGGGGGTTAGACCCAATATCAGGAGACTAGGAAGGAGGAGGCCTAA GGATGGGGCTTTTCTGTCACCAATCCTGTCCCTAGTGGCCCCACTGTGGGGTGGAGGGG.

Next, Cal27-Cas9 cells were infected with Human Kinome CRISPR pooled library (Brunello, RRID:Addgene_75312) at representation of 650 and a multiplicity of infection (MOI) of 0.3. The viral titer of lentivirus was analyzed using qRT-PCR-titer kit (#631235, Takara, Mountain View, CA), and functional titration. Human Kinome CRISPR pooled library (Brunello) was a gift from John Doench & David Root (RRID:Addgene_75312). Cal27-Cas9-kinome library cells were treated with 2 different groups; vehicle treated or INK128 (10nM) treated group, with triplicate. For PD 0 and PD 20 samples, the barcode was PCR-recovered from genomic samples, and samples where sequenced to calculate abundance of the different sgRNA probes. PCR of sgRNA for Illumina sequencing protocol was obtained from the Broad Institute (https://portals.broadinstitute.org/gpp/public/resources/protocols). The change in the relative abundance of each sgRNA in the library over time is measured using PinAPL-Py software (15). Significantly changed hit sgRNAs were extracted with adjusted p value < 0.001. The hit sgRNAs were subjected to pathway analysis using Enrichr software (16). KEGG pathway combined score was calculated with p-value and z score as follows; $c = \log(p) * z$, where c = the combined score, p = Fisher exact test p-value, and z = z-score (17). Next generation sequencing was conducted by IGM (Institute for Genomic Medicine) Genomics center in UC San Diego. Sequencing data from the CRISPR screen was deposited into SRA (BioProject ID: PRJNA1119544).

Antibodies. Antibodies against CCND1 (Cell Signaling Technology Cat# 2978, RRID:AB_2259616) , CCNE1 (Cell Signaling Technology Cat# 20808, RRID:AB_2783554), pRb (Cell Signaling Technology Cat# 9307, RRID:AB_330015), Rb (Cell Signaling Technology Cat# 9309, RRID:AB_823629), pS6 (Cell Signaling Technology Cat# 2211, RRID:AB_331679), S6 (Cell Signaling Technology Cat# 2217, RRID:AB_331355), pERK (Cell Signaling Technology Cat# 4370, RRID:AB_2315112), ERK (Cell Signaling Technology Cat# 9102, RRID:AB_330744), pAKT (Cell Signaling Technology Cat# 4060, RRID:AB_2315049), AKT (Cell Signaling Technology Cat# 9272, RRID:AB_329827), CDK4 (Cell Signaling Technology Cat# 12790, RRID:AB_2631166), eIF4E (Cell Signaling Technology Cat# 9742, RRID:AB_823488), Cas9 (Cell Signaling Technology Cat# 14697, RRID:AB_2750916), HA-Tag (Cell Signaling Technology Cat# 3724, RRID:AB_1549585), vinculin (Cell Signaling Technology Cat# 13901, RRID:AB_2728768), β-Actin (Cell Signaling Technology Cat# 4967, RRID:AB_330288) and GAPDH (Cell Signaling Technology Cat# 2118, RRID:AB_561053) were purchased from Cell Signaling Technology (Beverly, MA, USA). Antibody against eIF4G (Santa Cruz Biotechnology Cat# sc-133155, RRID:AB_2095748) and CDK6 (Santa Cruz Biotechnology Cat# sc-177-G, RRID:AB_631226) were purchased from Santa Cruz Biotechnology (Dallas, TX, USA). CCND1 (Proteintech Cat# 26939-1-AP, RRID:AB_2880691) and CCNE1 (Proteintech Cat# 11554-1-AP, RRID:AB_2071066) were purchased from Proteintech (Rosemont, IL, USA). BrdU (Bio-Rad Cat# OBT0030S, RRID:AB_609570) was purchased from Bio-Rad (Hercules, CA, USA).

DNA constructs and viral infection. pBABE puro cyclinD1 HA was a gift from William Hahn (Addgene plasmid # 9050; RRID:Addgene_9050). pInducer20 Cyclin E1 was a gift from Jean Cook (Addgene plasmid # 109348; RRID:Addgene_109348). Plasmids were packaged into retrovirus and lentivirus in HEK293T cells respectively, and cells were infected with viruses for 2 days. The infected cells were selected with puromycin (1 μg/mL) for 3 days, or selected with G418 (1000 μg/mL) for 7 days, respectively. To overproduce CCNE1, cells were treated with 1 μg/mL doxycycline for at least 48 hours.

siRNA and transfection. SMARTpool si-CDK4 (#L-003238-00-0005) and si-CDK6 (#L-003240-00-0005) were purchased from Dharmacon. siRNA Universal Negative Control #1 (#SIC-001) was from Sigma-Aldrich. All cells were transfected using Lipofectamine® RNAiMAX Reagent (#13778075, Invitrogen) and OPTI-MEM (#31985062, Gibco) according to the manufacturer's instructions. siRNA transfection was performed as previously described (13,18).

Cell viability assay. 3000 cells were seeded in 96 well plates, and treated as indicated after they attach to the plates. After treatment for 72 hours, culture medium was supplemented with 1/100 of the culture volume of Aquabluer reagent (#6015, MultiTarget Pharmaceuticals LLC, Colorado Springs, CO, USA) for 1h to 4h. Absorbances were recorded at 570 nm in a Biotek Synergy Neo microplate reader.

Synergy determination with the Chou-Talalay method and the Bliss delta score. The Chou–Talalay method was used to determine possible synergistic effects of selected drugs combinations (19). 3,000 cells per well were seeded in 96-well plates. Cells were treated with either single inhibitors or combinations thereof using seven different dilutions of each inhibitor and in technical triplicates. Cell viability was measured, after 72-hour treatment, with the AquaBluer Cell Viability Reagent (#6015, MultiTarget Pharmaceuticals LLC) with Tecan SPARK Multimode Microplate Reader (RRID:SCR_021897). Combination index (CI) values showing either synergy (<1) or antagonism (>1) were calculated using the Chou–Talalay method. The Bliss independence model assumes a stochastic process in which two drugs elicit their effects independently, and the expected combination effect was calculated using the following

equation: IAB= IA + IB – IA x IB, where IA and IB are the single-agent inhibition levels at fixed concentrations (20). If the experimentally measured effect of the drug combination was equal to, higher than, or lower than the expected effect (IAB), the combination was additive (ΔBliss= 0), synergistic (<0), or antagonistic (>0), respectively.

Orosphere assay. Cells were seeded in 24-well ultra-low attachment culture plates (Corning, Corning, NY) at 500 cells per well. Medium consisted of DMEM/F12 Glutamax supplement medium (#10565042, Thermo Fisher Scientific), basic fibroblast growth factor (bFGF: 20 ng/ml, #13256029, Thermo Fisher Scientific), epithelial growth factor (EGF: 20 ng/ml, #PHG0313, Thermo Fisher Scientific), B-27 (1:50 dilution, #17504044, Thermo Fisher Scientific), and N2 supplement (1:100 dilution, #17502-048, Thermo Fisher Scientific). Vehicle, INK128 (20 nM), or palbociclib (0.4 μM) were added when cells were seeded. Around ten days after seeding, photographies were obtained, and the sizes of sphere colonies on each well were counted using a microscope.

Colony formation assay. 1,000 cells per well were seeded in 12-well plates and Vehicle, INK128 (20 nM) and/or palbociclib (0.4 μM) were added after they were attached. For 8-10 days treatment, the medium was changed every 2-3 days. Cell culture plates containing colonies were gently washed with PBS twice and fixed for 5 minutes with methanol/acetic acid solution (3:1) and stained for 15minutes with 0.5% crystal violet solution diluted in methanol. Excess stain was removed by washing repeatedly with PBS. The colony area percentage was calculated using ImageJ.

RNA isolation from HNSCC cells, and quantitative PCR. HNSCC cells were treated with INK128 (30 nM) and/or palbociclib (0.6 μM) for 24 hours. RNA was extracted from cells using RNeasy Plus kit (#74134, QIAGEN). Total RNA was converted to cDNA using SuperScript™ VILO™ cDNA Synthesis Kit (#11754250, ThermoFisher Scientific). qPCR was performed using PowerUp SYBR™ Green Master Mix (#A25742, ThermoFisher Scientific). mRNA levels were normalized by RPS18 expression. The following primers were used for qPCR. CCND1 fwd 5'-AGCTGTGCATCTACACCGAC, CCND1 rev5'- GAAATCGTGCGGGGTCATTG, CCNE1 fwd5'-CCATCATGCCGAGGGAGC, CCNE1 rev5'- GGTCACGTTTGCCTTCCTCT, RPS18 fwd5'-AGTCCCTGCCCTTTGTACACA, RPS18 rev5'- CGATCCGAGGGCCTCACTA.

RNA immunoprecipitation (RIP) assay. HNSCC cells were treated with INK128 (30 nM) and/or palbociclib (0.6 μM) for 24 hours, and cell lysates were collected. RIP assay was performed using EZ-Magna RIP RNA-binding Protein Immunoprecipitation Kit (Sigma-Aldrich, #17-701) following the manufacturer's instructions. Antibody against eIF4G (Santa Cruz Biotechnology Cat# sc-133155, RRID:AB_2095748) was used for the part of immunoprecipitation and mouse IgG antibody (Cell Signaling Technology Cat# 5415, RRID:AB_10829607) was used for isotype control. cDNA synthesis of input RNA and eIF4G binding RNA were followed by qPCR.

Western blotting. Exponentially growing cells were washed in cold PBS, lysed on ice in lysis buffer (50 mM Tris-HCl, 150 mM NaCl, 1 mM EDTA, 1% NP-40, supplemented with Halt™ Protease and Phosphatase Inhibitor Cocktail (#78440, ThermoFisher Scientific). Cell extracts were collected, sonicated, and centrifuged to remove the cellular debris. Supernatants containing the solubilized proteins were quantified using the detergent compatible DC protein assay kit (#5000111, Bio-Rad, Hercules, CA, USA). Equal amounts of protein were separated by SDS-PAGE, and transferred to PVDF membranes. For immunodetection, membranes were blocked for 20 min at room temperature in 5% non-fat dry milk in TBST buffer, followed by 2h

incubation with the appropriate antibodies, in 3% BSA-T-TBS buffer. Detection was conducted by incubating the membranes with horseradish peroxidase–conjugated goat anti-rabbit IgG secondary antibody (Southern Biotech, Birmingham, AL, USA) at a dilution of 1:20,000 in 5% milk-T-TBS buffer, at room temperature for 40 min, and visualized with Immobilon Western Chemiluminescent HRP Substrate (EMD Millipore, Burlington, MA, USA).

Immunoprecipitation. HNSCC cells were treated with INK128 (30nM) for 24 hours, and cell lysates were collected. Immunoprecipitation was performed using Pierce classic magnetic IP/Co-IP Kit (Thermo Scientific, #88804) following the manufacturer's instructions. The input proteins and IP products were analyzed for indicated proteins by western blotting.

Animal work. All the mice studies were approved by the Institutional Animal Care and Use Committee (IACUC), University of California, San Diego (protocol #S15195). To establish tumor xenografts, 2.0×10^6 cells were transplanted into the flanks of athymic nude mice (female, four to six weeks old) (Charles River Laboratories, Wilmington, MA), and when the tumor volume reached approximately 200 mm^3, the mice were randomized into groups and treated by intraperitoneal injection (ip) with INK128 (1 mg/kg/day, five times a week) or oral gavage with palbociclib (50mg/kg/day, five times a week), or control diluent (10 tumors per each group). Tumor volume was calculated by using the formula length × width × width/2. The mice were euthanized at the indicated time points and tumors isolated for histologic and immunohistochemical evaluation.

Immunohistochemistry staining. All samples were fixed in zinc formalin (Z-Fix) and embedded in paraffin; 5 μm sections were stained with Hematoxylin-Eosin for diagnostic purposes. For immunohistochemistry (IHC) studies, samples were deparaffinized, hydrated with graded ethanol, and the endogenous peroxidase was blocked with 3% H_2O_2 in 70% ethanol. After washing with distilled water, antigen retrieval was performed with IHC antigen retrieval solution (#00-4955-58, Invitrogen) in a microwave at the high setting. Slides were then washed with water and PBS, and incubated with the primary and secondary antibodies, and developed with the Elite® ABC kit (Vector Laboratories, #PK-6100) and the ImmPACT DAB substrate kit (Vector Laboratories, #SK-4105). The following antibodies were used: BrdU (Bio-Rad Cat# OBT0030S, RRID:AB_609570, 1:50), pS6 (Cell Signaling Technology Cat# 2211, RRID:AB_331679, 1:300), p4EBP1 (Cell Signaling Technology Cat# 2855, RRID:AB_560835, 1:800), CCND1 (Proteintech Cat# 26939-1-AP, RRID:AB_2880691, 1:800) and CCNE1 (Proteintech Cat# 11554-1-AP, RRID:AB_2071066, 1:400). Samples were scanned with Aperio AT2 microscope slide scanner (Leica) and analyzed using QuPath software.

Genomic data analysis. mRNA and RPPA expression analyses where performed using publicly available data generated by The Cancer Gene Atlas consortium, accessed through cBioportal (www.cbioportal.org) (21,22) .

Statistical analysis. All data analysis was performed using GraphPad Prism9 for MacOS (GraphPad Software, San Diego, CA, USA). Comparisons between experimental groups were made using one-way ANOVA with Tukey's post hoc test or two-way ANOVA with Tukey's post hoc test. Overall survival curves were plotted according to Kaplan–Meier method and compared by log-rank test. Asterisks denote statistical significance (non-significant or NS, $P > 0.05$; *$P < 0.05$; **$P < 0.01$; ***$P < 0.001$ and ****$P < 0.0001$). All data are reported as mean ± standard error of the mean (SEM) with at least two biologically independent replicates. The detailed statistic for each plot was described in figure legends.

Data Availability. The CRISPR screening data generated in this study are publicly available in Sequence Read Archive (SRA) at BioProject ID: PRJNA1119544.

Results

CRISPR/Cas9 screening identifies cell cycle regulation as a synthetic lethal mechanism for mTORi in HNSCC

To explore synthetic lethal targets and resistance mechanisms for mTORi in HNSCC, we took advantage of CRISPR screening. First, we generated Cas9-expressing Cal27 HNSCC cells (Cal27-Cas9) (Supplementary Fig. S1A) and confirmed cutting efficiency using two different sgRNAs (gT1/ gT2) targeting AAVS locus. Next generation sequencing (NGS) for these cells showed 83.0% and 98.3% of non-homologous end joining (NHEJ) frequency for gT1 and gT2, respectively (Supplementary Fig. S1B), indicating the cutting efficiency for Cal27-Cas9 was suitable to conduct the planned screening. Since our purpose was to identify druggable targets, and the kinome is the target of a large proportion of oncology-related drugs, we used a human kinome-wide CRISPR library, targeting 763 genes consisting of 4 sgRNAs for each gene (23). After infecting Cal27-Cas9 cells with the kinome-wide CRISPR library, we treated Cal27-Cas9-kinome cells with vehicle or mTORi until total population doubling reached 20 (Fig.1A and Supplementary Fig. S1C). In this study, we applied INK128 (also known as MLN-0128 and TAK-228), which is an mTOR ATP-competitive small molecule inhibitor, and reported to have excellent physiochemical properties (24,25). After extracting DNA from these cells, we performed PCR to amplify the barcodes, and NGS to identify depleted sgRNAs in mTORi-treated cells compared with vehicle-treated cells (Fig. 1A). Quality control analysis of the sgRNA screen is shown in Supplementary Fig. S1D and S1E, and the configuration of PinAPL-Py software used is included in Supplementary Table S1.

We show all dropout-sgRNAs in Figure 1B and Supplementary Table S2. As a specificity control, none of the 98 non-targeting sgRNA revealed any significant changes when comparing the control and INK128 treated cells (Supplementary Table S3). Next, hits with significant p-values less than 0.01 were selected, and 109 sensitizing hits were identified (Fig. 1C and Supplementary Table S4). Remarkably, the most depleted gene was mTOR, which is consistent with the fact that we used a low dose mTORi to identify synthetic lethal targets (Fig. 1D). We next applied pathway analysis for hit sgRNAs not only focusing on single sgRNAs but investigating hit sgRNAs as an integrated set of genes to find effective pathways to target. The 109 sensitizing hits set was analyzed with KEGG pathway analysis using Enrichr (https://maayanlab.cloud/Enrichr/) (26) (Fig. 1E and Supplementary Table S5). The results revealed significant enrichment of ErbB signaling pathway and MAPK signaling pathway. Aligned with these findings, co-targeting ErbB signaling with mTORi for HNSCC has been investigated (27,28), including our combination study of cetuximab and rapamycin or everolimus (29), and our group reported by RNAi screening that MAPK signaling is synthetic lethal with first generation mTORi (rapamycin) (30). Of interest, we also found a highly significant enrichment of Cell cycle pathways (Fig. 1E). As progression through the cell cycle is regulated by cyclins and cyclin dependent kinases (CDKs), we first analyzed the association between cyclin expression and prognosis of HNSCC using TCGA data. The high mRNA and protein expression of Cyclin D1, which is encoded by the *CCND1* gene, is a worse prognostic factor for overall survival in HNSCC patients (Fig. 1F and 1G), supporting an important role of cell cycle signaling for HNSCC. These results prompted us to explore the possibility of co-targeting cell cycle mechanisms and mTOR signaling in HNSCC.

Combination of INK128 and palbociclib shows strong synergism in HNSCC cells *in vitro*

Although targeting CCND1 gene and protein levels may represent a therapeutic option in HNSCC, this may not be currently feasible, and instead we focused on targeting their associated kinases, CDKs, as CDK inhibitors are already approved for other indications thereby enhancing the translational potential of our studies. We first investigated the inhibitory effects of siRNA knockdown of CDK4 and CDK6, which are strongly associated with cyclin D (Supplementary Fig. S2A). Considering the enhanced clinical response of HPV- HNSCC patients (8), for these studies, we used representative HPV- HNSCC cells (Cal27 and HN12). These cells harbor typical *TP53* mutations and exhibit persistent mTOR activation in the absence of *PIK3CA* mutations and *PTEN* genomic alterations that are more frequent in HPV+ HNSCC lesions, thus reflecting the human HPV- HNSCC oncogenome (10). Knockdown of CDK4 and/or CDK6 reduced cell viability only partially in HNSCC cells (Fig. 2A), which was increased by INK128 treatment. In this regard, individual CDK4 and CDK6 knockdown had limited impact on the response to INK128, but their growth suppressive activity was significantly increased when the knockdown of both kinases was combined (Fig. 2A). This likely redundancy may explain why these kinases were not initially identified individually as targets in our CRISPR screen. In turn, these observation provided an opportunity to investigate the use of palbociclib, an FDA-approved cell cycle-targeted agent that can specifically inhibit CDK4/CDK6, to block cell cycle signaling in combination with mTORi, and specifically in HPV- HNSCC cells as HPV-positive cells are refractory to CDK inhibition due to the viral oncoprotein E7 causing Rb degradation (31).

INK128 potently blocked the cell viability with growth inhibition of 50% (GI_{50}) of 42 nM for Cal27 cells (Fig. 2B), GI_{50} for palbociclib was 1.27 μM for Cal27 cells (Fig. 2C). Similarly, The GI_{50} for INK128 in HN12 was 28 nM, and 0.85 μM for palbociclib (Supplementary Fig. S2B and S2C). Next, we investigated the synergism between these drugs by the Chou-Talalay method (19). Fraction affected combination index (CI) plot showed CI of below 1 for most percentage of fraction when cells were treated with 1:10 or 1:20 concentrations of INK128 and palbociclib, respectively (Fig. 2D). These data suggest strong synergistic effect of this combination. Also, we performed a factorial dose matrix combinatorial drug treatment with INK128 and palbociclib, supporting synergism for this combination (Fig. 2E). Furthermore, we analyzed synergism using Bliss model (20), which suggested strong synergism with relatively higher INK128 concentration than GI_{50} (Fig. 2F). To confirm the synergism in another cell line, we used HN12 HNSCC cells. The combination index was below 1 when used 1:10 or 1:20 concentration of INK128 and palbociclib respectively, similar as Cal27 cells (Supplementary Fig. S2D). To further confirm the efficacy of combination therapy, we performed a colony formation assay and found that combination therapy significantly inhibited colony growth compared to treatment with INK128 or palbociclib alone (Fig. 2G and Supplementary Fig. S2E). To analyze the combination effect in conditions which are more reflective of cell growth in 3D, *in vivo* conditions, we tested orosphere assays which allows for the propagation of cancer cells that retained stemness and self-renewal (32). INK128 and palbociclib significantly reduced the size of sphere formation in Cal27 and HN12 cells, and co-administration of these two drugs could significantly block the sphere formation (Fig. 2H and Supplementary Fig. S2F). These data suggest the possibility of using the combination of INK128 and palbociclib for treatment of HNSCC.

Upregulation of CCNE1 by palbociclib confers resistance to palbociclib, which can be reverted by INK128

To investigate the mechanism for the synergism between INK128 and palbociclib in HNSCC, we explored changes in signaling components and cell cycle mechanisms. Based on our resuls above, we first focused on CCND1 and CCNE1 associated with CDK4/6. qPCR result showed that *CCND1* and *CCNE1* mRNA expression were significantly increased by palbociclib

treatment in Cal27 and HN12 (Fig. 3A and Supplementary Fig. S3A). On the other hand, *CCND1* and *CCNE1* expression were significantly decreased with INK128 alone and combination treatment. Next, we performed Western blotting to exam the protein expression. As expected, INK128 could effectively inhibit PI3K/ mTOR activation as judged by pAKT and pS6 expression levels in Cal27 and HN12 (Fig. 3B and Supplementary Fig. S3B). As for cell cycle, INK128 increased phosphorylation of retinoblastoma protein (RB) and decreased CCND1 expression. While INK128 suppresses the AKT/mTOR pathway, it promotes RB phosphorylation and activates cell cycle pathways. In contrast, palbociclib treatment prevented phosphorylation of RB, and caused upregulation of CCND1 and CCNE1. We hypothesized CCND1 and CCNE1 activation could represent a mechanism for palbociclib resistance in HNSCC, considering recent clinical data showing high *CCNE1* as worse clinical outcome for palbociclib treated patients in breast cancer (33,34). In this regard, we engineered HNSCC cell lines which stably overexpress CCND1 and CCNE1 individually, and together (Supplementary Fig. S3C). This approach revealed increased resistance to palbociclib in Cal27-CCNE1 cells compared with Cal27-wt cells (Fig. 3C). However, no significant resistance to palbociclib was observed in Cal27-CCND1 cells. CCND1/E1-overxpressing Cal27 cells were also resistant, however, the resistance was similar as CCNE1-Cal27 cells, which suggests that no additional resistance was conferred by CCND1 overexpression. Similar results were confirmed using HN12-wt, HN12-CCND1, HN12-CCNE1, and HN12-CCND1/E1 and palbociclib (Supplementary Fig. S3D). These data indicate that CCNE1 overexpression may represent one of the mechanisms of resistance to palbociclib in HNSCC.

Remarkably, although we observed upregulation of CCNE1 after treatment with palbociclib in HNSCC cells, the addition of INK128 together with palbociclib could revert this overexpression and downregulated CCNE1 (Fig. 3B and Supplementary Fig. S3B). Furthermore, the resistance of Cal27-CCNE1 and HN12-CCNE1 to palbociclib in terms of cell viability was completely abolished by addition of INK128 (Fig. 3D and Supplementary Fig. S3E). These results indicate that INK128 treatment suppresses palbociclib-induced CCNE1 elevation and prevents resistance acquisition. To gain a mechanistic insight into this process, we built on our previous observations that blockade of mTOR by INK128 leads to dephosphorylation of 4E-BP1, which in turn reduces eIF4E and eIF4G binding, resulting in reduced mRNA translation of proliferating proteins (24). This was confirmed in the present study (Supplementary Fig. S3F). Next, we performed RNA immunoprecipitation (RIP) assays to directly investigate the binding of endogenous eIF4G to *CCND1* and *CCNE1* mRNAs. Indeed, INK128 treatment reduced the binding of eIF4G to *CCNE1* mRNA in Cal27 and HN12 cells (Fig. 3E and Supplementary. Fig. S3G). Binding of eIF4G to *CCND1* mRNA was reduced by INK128 treatment in Cal27, but not in HN12 (Fig. 3F and Supplementary. Fig. S3H), which suggests a cancer heterogeneity in this response and a more general impact on *CCNE1*. On the other hand, palbociclib significantly increased binding of eIF4G to the mRNA for *CCND1* and *CCNE1* in both Cal27 and HN12 cells. Thus, we hypothesized INK128 could revert the overexpression of CCNE1 caused by palbociclib treatment by reducing binding of eIF4G and *CCNE1*. As shown in Fig. 3E and Supplementary. Fig. S3G, combination treatment with INK128 and palbociclib potently reduced *CCNE1* mRNA binding to eIF4G compared with control or palbociclib treatment. These data suggest that CCNE1 activation or overexpression represents one of the resistance mechanisms to palbociclib, and that mTOR acts upstream of CCNE1, controlling its mRNA translation (Fig. 3G). Together, these data provide a rationale for the combination therapy of INK128 and palbociclib for HNSCC.

Combination therapy with INK128 and palbociclib is effective against HNSCC xenograft

Next, we asked if this combination of INK128 and palbociclib is effective *in vivo*. Using Cal27 and HN12 xenograft models, we started treatment with INK128, palbociclib, or combination after tumors were established. Since high frequency of myelosuppression has been reported for palbociclib in clinical trials (35), we used relatively low dose palbociclib for this in vivo study. In our Cal27 xenograft model, INK128 or palbociclib treatment as a single agent did not inhibit tumor growth, but the combination of these drugs significantly inhibited tumor growth (Supplementary Fig. S4A). As for HN12 xenograft, palbociclib did not inhibit tumor growth, and INK128 was relatively effective as a single agent, but combination therapy had significantly stronger effect than single agents (Fig. 4A). The H&E staining of these tumors showed that mTOR inhibition together with palbociclib caused tumor collapse with smallest residual tumor masses at the end of the treatment (Fig. 4B and Supplementary Fig. S4B). To assess the inhibition of proliferation *in vivo*, we used BrdU staining for tumors with short-term treatment of palbociclib, INK128, or combination. The combination therapy demonstrated the lowest percentage of BrdU positive cells in both Cal27 and HN12 xenograft which indicate strong inhibition of cell proliferation in co-administered tumors (Fig. 4C and Supplementary Fig. S4C). In addition, we used immunohistochemistry to confirm protein expression in the tumors (Fig. 4D and Supplementary Fig. S4D). INK128 treatment decreased expression of phospho-S6 and phospho-4EBP1, and palbociclib treatment increased the expression of CCND1 and CCNE1. In contrast, these increases were suppressed by INK128 in the combination treatment. Furthermore, despite only five days of treatment, combination therapy induces tumor collapse (Supplementary Fig. S4D). These results indicate that even in vivo, the cyclin upregulation induced by palbociclib is rescued by mTORi, thereby displaying a strong synergistic effect.

Discussion

The frequent genomic alterations in *CDKN2A* and *CCND1* in HPV-negative clinical HNSCC cases suggest that there is a strong rationale to target CDK4/6 to inhibit tumor progression in HNSCC. Several selective CDK4/6 inhibitors are available in the clinic, such as abemaciclib, ribociclib, and palbociclib. Among them, palbociclib is the first FDA-approved CDK4/6 specific inhibitor, inducing G1 arrest, with a concomitant reduction of phosphorylation of the Rb protein (36). It is approved for advanced or metastatic hormone receptor-positive (HR+) and human epidermal growth factor receptor 2-negative (HER2-) breast cancer (BCa), in combination with endocrine therapy (34,37). For HPV-negative HNSCC, several clinical trials have been conducted using CDK4/6 inhibitors. In selected patients with *CDKN2A*-altered HNSCC, palbociclib monotherapy showed modest antitumor activity (4). Also, in the PALATINUS study, the combination of palbociclib and cetuximab did not prolong the OS in unselected patients (5). To strengthen the anti-tumor activity of palbociclib in HNSCC, novel strategies are needed. In the subgroup analysis in PALATINUS patients, trends for better OS were observed in patients with *CDKN2A* mutations or CDK4/6 amplification, but in the absence of *PIK3CA* alterations (5). Consistent with these data, basic studies showed that *PIK3CA*-mutant HNSCC cells are less responsive to palbociclib (38). These results are consistent with the results of our study showing that mTORi and palbociclib could have beneficial combinatory effects on HNSCC.

The therapeutic potential of mTORi for HNSCC has been extensively studied. Our group pioneered the use of rapamycin as a single agent to treat HNSCC xenograft (6). In this early study, we showed that phosphorylated S6, the most downstream target of the Akt-mTOR pathway, is frequently accumulated in HNSCC clinical specimens. Furthermore, we used rapamycin to treat four different types of HNSCC xenografts, resulting in tumor regression. Following this study, several groups have reported the effectiveness of mTORi for HNSCC (39-

41). In turn, these analyses from basic research led to multiple clinical trials including single agent mTORi, or combined treatment with mTORi and other agents (9,42-45). Our group has recently shown the efficacy of rapamycin as monotherapy for previously untreated patients. 21 days treatment for 16 patients with rapamycin resulted in 1 complete response, 3 partial response, and 12 stable disease, supporting the potential role of mTORi for HNSCC (7). Furthermore, clinical trials with administration of metformin, which has been shown to regulate mTOR via AMPK, to premalignant lesions of HNSCC has been conducted, and it shows promising results as judged by pathological responses (46). Similarly, we have recently shown that mTOR inhibition with everolimus in the adjuvant setting after definitive treatment of locally advanced HNSCC lesions reduces significantly tumor relapse, specifically in HPV negative cases (8). However, a clinical trial targeting mTOR in heavily pretreated HNSCC patients did not show clinical benefit with everolimus (9). These findings suggest that previous treatments may cause genetic alterations and epigenetic changes in cancer cells; consequently, more complicated mechanisms driving cell growth may be active in these lesions when compared to the use of mTORi in newly diagnosed HNSCC cases, or as an adjuvant post-surgery and/or radiation. In addition, in these early clinical trials mainly three mTORi were used; rapamycin (sirolimus), everolimus and temsirolimus. These three mTORi are often referred as first generation mTORi, blocking only mTORC1. In our study, we used INK128, which is a second generation mTORi that binds to the ATP-binding site of mTOR and inhibits the catalytic activity of both mTORC1 and mTORC2 without inhibiting other kinases (25). In this regard, INK128 is different from previous mTORi, and the anti-tumor effect of second generation mTORi is promising (47).

To overcome potential mechanisms limiting the response to mTORi, we hypothesized that the administration of mTORi to HNSCC combined with targeting agents suppressing resistance pathways may provide better outcomes. In this study, we applied an unbiased approach to find synthetic lethal and resistance targets for INK128 and showed that the cell cycle pathway can be a synthetic lethal target with INK128. Xenograft experiments using human HNSCC cells showed promising results with the co-administration of INK128 and palbociclib. Mechanistically, we showed that INK128 could inhibit the adaptive accumulation of CCNE1 caused by palbociclib. Since INK128 blocks mTORC1 and mTORC2, it can inhibit phosphorylation of 4E-BP1 strongly, which in turn reactivates the tumor suppressive activity of 4E-BP1 (24,25). Dephosphorylated 4E-BP1 associates with eIF4E, and inhibits binding between eIF4E and eIF4G, resulting in reduced translation of mRNAs that are essential to cell proliferation for tumor (24). In this case, one of the eIF4G-biding mRNAs reduced by INK128 is *CCNE1*. This may explain the reduced level of CCNE1 protein after INK128, and the efficacy of combination therapy with INK128 and palbociclib (see Fig. 5).

Our findings may now provide a mechanistic framework on how the interplay between CDK4/CDK6 blockade and mTORi can result in increased tumor control and prevent the acquisition of palbociclib resistance. Aligned with this perspective, recent studies suggest that enhanced *CCNE1* mRNA expression levels in BCa patients are associated with resistance to palbociclib (33,48), which was recapitulated by our current findings supporting that CCNE1 overexpression is sufficient to induce palbociclib resistance in HNSCC cells. Similarly, the PI3K/mTOR pathway was found to be overactivated in palbociclib-resistant breast cancer cells, with increased levels of cyclin D1 and CDK4 translation that could be reverted by PI3K/mTOR inhibition (49), and palbociclib-based high-throughput combination drug screens showed a significant synergistic effect when palbociclib was combined with PI3K, EGFR, or MEK inhibitors in HNSCC (50). Furthermore, in *PIK3CA* mutant HNSCC cells a combination of a PI3K/mTOR inhibitor and palbociclib was reported to be effective xenograft tumors (38), albeit by a poorly understood mechanism. These results support that the use of palbociclib alone has limited

activity in HNSCC likely due to the rapid acquisition of adaptive resistance through a positive feedback loop resulting in increased CCNE1 expression, which can be prevented by the concomitant mTOR pathway blockade (see Fig. 5).

In summary, our unbiased genetic library screen approach revealed that concomitant mTOR blockade reverts the adaptive resistance to palbociclib. Specifically, CCNE1 overexpression caused by palbociclib can be abolished by co-administration of INK128. Ultimately, our findings may provide a novel strategy for HPV negative HNSCC patients by co-targeting mTOR and key cell cycle regulating molecules, which can also have an impact in multiple cancer types that fail to respond to CDK4/6 inhibitors as single agents.

Acknowledgments

Y.G. is supported by the JSPS Overseas Research Fellowships, the Uehara Memorial Foundation Research Fellowship, and the SGH Foundation Cancer Research Fellowship.

K.K. is supported by the JSPS Overseas Research Fellowships, the Uehara Memorial Foundation Research Fellowship and Study abroad support of Mochida Memorial Foundation for Medical and Pharmaceutical Research.

Y.G. initiated the study; Y.G. K.K. and J.S.G. designed the study and experiments; Y.G., X.W., N.A, K.F., M.A., and A.K. performed the CRISPR screening; Y.G., K.K., T.A., H.I., K.S., T.I. and X.F. performed *in vitro* and *in vivo* experiments, Y.G., K.K., T.A., N.A. and J.S.G. prepared the manuscript, Z.W., N.A., P.M. and J.S.G. provided advice and supervised the project. All authors discussed the results and reviewed the manuscript.

All cartoon renderings were created with the BioRender online platform (BioRender.com).

References

1. Siegel RL, Miller KD, Wagle NS, Jemal A. Cancer statistics, 2023. CA: a cancer journal for clinicians **2023**;73:17-48
2. Gutkind JS, Bui JD. The Next Frontier: Head and Neck Cancer Immunoprevention. Cancer Prev Res (Phila) **2017**;10:681-3
3. Comprehensive genomic characterization of head and neck squamous cell carcinomas. Nature **2015**;517:576-82
4. Pisick EP, Rothe M, Mangat PK, Garrett-Mayer L, Worden FP, Bauman JR*, et al.* Palbociclib (P) in patients (pts) with head and neck cancer (HNC) with CDKN2A loss or mutation: Results from the Targeted Agent and Profiling Utilization Registry (TAPUR) study. Journal of Clinical Oncology **2021**;39:6043-
5. Adkins DR, Lin JC, Sacco A, Ley J, Oppelt P, Vanchenko V*, et al.* Palbociclib and cetuximab compared with placebo and cetuximab in platinum-resistant, cetuximab-naïve, human papillomavirus-unrelated recurrent or metastatic head and neck squamous cell carcinoma: A double-blind, randomized, phase 2 trial. Oral Oncol **2021**;115:105192
6. Amornphimoltham P, Patel V, Sodhi A, Nikitakis NG, Sauk JJ, Sausville EA*, et al.* Mammalian target of rapamycin, a molecular target in squamous cell carcinomas of the head and neck. Cancer Res **2005**;65:9953-61

7. Day TA, Shirai K, O'Brien PE, Matheus MG, Godwin K, Sood AJ, *et al.* Inhibition of mTOR Signaling and Clinical Activity of Rapamycin in Head and Neck Cancer in a Window of Opportunity Trial. Clinical cancer research : an official journal of the American Association for Cancer Research **2019**;25:1156-64
8. Nathan CO, Hayes DN, Karrison T, Harismendy O, Flores JM, Moore-Medlin T, *et al.* A Randomized Multi-institutional Phase II Trial of Everolimus as Adjuvant Therapy in Patients with Locally Advanced Squamous Cell Cancer of the Head and Neck. Clinical cancer research : an official journal of the American Association for Cancer Research **2022**;28:5040-8
9. Geiger JL, Bauman JE, Gibson MK, Gooding WE, Varadarajan P, Kotsakis A, *et al.* Phase II trial of everolimus in patients with previously treated recurrent or metastatic head and neck squamous cell carcinoma. Head & neck **2016**;38:1759-64
10. Martin D, Abba MC, Molinolo AA, Vitale-Cross L, Wang Z, Zaida M, *et al.* The head and neck cancer cell oncogenome: a platform for the development of precision molecular therapies. Oncotarget **2014**;5:8906-23
11. Doench JG. Am I ready for CRISPR? A user's guide to genetic screens. Nature reviews Genetics **2018**;19:67-80
12. Paradis JS, Acosta M, Saddawi-Konefka R, Kishore A, Gomes F, Arang N, *et al.* Synthetic Lethal Screens Reveal Cotargeting FAK and MEK as a Multimodal Precision Therapy for GNAQ-Driven Uveal Melanoma. Clinical cancer research : an official journal of the American Association for Cancer Research **2021**;27:3190-200
13. Arang N, Lubrano S, Rigiracciolo DC, Nachmanson D, Lippman SM, Mali P, *et al.* Whole-genome CRISPR screening identifies PI3K/AKT as a downstream component of the oncogenic GNAQ-focal adhesion kinase signaling circuitry. The Journal of biological chemistry **2022**;299:102866
14. Pinello L, Canver MC, Hoban MD, Orkin SH, Kohn DB, Bauer DE, *et al.* Analyzing CRISPR genome-editing experiments with CRISPResso. Nature biotechnology **2016**;34:695-7
15. Spahn PN, Bath T, Weiss RJ, Kim J, Esko JD, Lewis NE, *et al.* PinAPL-Py: A comprehensive web-application for the analysis of CRISPR/Cas9 screens. Scientific reports **2017**;7:15854
16. Kuleshov MV, Jones MR, Rouillard AD, Fernandez NF, Duan Q, Wang Z, *et al.* Enrichr: a comprehensive gene set enrichment analysis web server 2016 update. Nucleic Acids Res **2016**;44:W90-7
17. Chen EY, Tan CM, Kou Y, Duan Q, Wang Z, Meirelles GV, *et al.* Enrichr: interactive and collaborative HTML5 gene list enrichment analysis tool. BMC bioinformatics **2013**;14:128
18. Feng X, Arang N, Rigiracciolo DC, Lee JS, Yeerna H, Wang Z, *et al.* A Platform of Synthetic Lethal Gene Interaction Networks Reveals that the GNAQ Uveal Melanoma Oncogene Controls the Hippo Pathway through FAK. Cancer cell **2019**;35:457-72 e5
19. Chou TC. Drug combination studies and their synergy quantification using the Chou-Talalay method. Cancer Res **2010**;70:440-6
20. Coppe JP, Mori M, Pan B, Yau C, Wolf DM, Ruiz-Saenz A, *et al.* Mapping phospho-catalytic dependencies of therapy-resistant tumours reveals actionable vulnerabilities. Nature cell biology **2019**;21:778-90
21. Gao J, Aksoy BA, Dogrusoz U, Dresdner G, Gross B, Sumer SO, *et al.* Integrative analysis of complex cancer genomics and clinical profiles using the cBioPortal. Science signaling **2013**;6:pl1
22. Cerami E, Gao J, Dogrusoz U, Gross BE, Sumer SO, Aksoy BA, *et al.* The cBio cancer genomics portal: an open platform for exploring multidimensional cancer genomics data. Cancer discovery **2012**;2:401-4

23. Doench JG, Fusi N, Sullender M, Hegde M, Vaimberg EW, Donovan KF*, et al.* Optimized sgRNA design to maximize activity and minimize off-target effects of CRISPR-Cas9. Nature biotechnology **2016**;34:184-91
24. Wang Z, Feng X, Molinolo AA, Martin D, Vitale-Cross L, Nohata N*, et al.* 4E-BP1 Is a Tumor Suppressor Protein Reactivated by mTOR Inhibition in Head and Neck Cancer. Cancer Res **2019**;79:1438-50
25. Feldman ME, Apsel B, Uotila A, Loewith R, Knight ZA, Ruggero D*, et al.* Active-site inhibitors of mTOR target rapamycin-resistant outputs of mTORC1 and mTORC2. PLoS biology **2009**;7:e38
26. Xie Z, Bailey A, Kuleshov MV, Clarke DJB, Evangelista JE, Jenkins SL*, et al.* Gene Set Knowledge Discovery with Enrichr. Curr Protoc **2021**;1:e90
27. Bozec A, Ebran N, Radosevic-Robin N, Sudaka A, Monteverde M, Toussan N*, et al.* Combination of mTOR and EGFR targeting in an orthotopic xenograft model of head and neck cancer. Laryngoscope **2016**;126:E156-63
28. Cassell A, Freilino ML, Lee J, Barr S, Wang L, Panahandeh MC*, et al.* Targeting TORC1/2 enhances sensitivity to EGFR inhibitors in head and neck cancer preclinical models. Neoplasia **2012**;14:1005-14
29. Wang Z, Martin D, Molinolo AA, Patel V, Iglesias-Bartolome R, Degese MS*, et al.* mTOR co-targeting in cetuximab resistance in head and neck cancers harboring PIK3CA and RAS mutations. Journal of the National Cancer Institute **2014**;106
30. Yamaguchi K, Iglesias-Bartolomé R, Wang Z, Callejas-Valera JL, Amornphimoltham P, Molinolo AA*, et al.* A synthetic-lethality RNAi screen reveals an ERK-mTOR co-targeting pro-apoptotic switch in PIK3CA+ oral cancers. Oncotarget **2016**;7:10696-709
31. Kalu NN, Johnson FM. Do CDK4/6 inhibitors have potential as targeted therapeutics for squamous cell cancers? Expert Opin Investig Drugs **2017**;26:207-17
32. Krishnamurthy S, Nör JE. Orosphere assay: a method for propagation of head and neck cancer stem cells. Head Neck **2013**;35:1015-21
33. Turner NC, Liu Y, Zhu Z, Loi S, Colleoni M, Loibl S*, et al.* Cyclin E1 Expression and Palbociclib Efficacy in Previously Treated Hormone Receptor-Positive Metastatic Breast Cancer. Journal of clinical oncology : official journal of the American Society of Clinical Oncology **2019**;37:1169-78
34. Guerrero-Zotano Á, Belli S, Zielinski C, Gil-Gil M, Fernandez-Serra A, Ruiz-Borrego M*, et al.* CCNE1 and PLK1 Mediate Resistance to Palbociclib in HR+/HER2- Metastatic Breast Cancer. Clin Cancer Res **2023**;29:1557-68
35. Sherr CJ, Beach D, Shapiro GI. Targeting CDK4 and CDK6: From Discovery to Therapy. Cancer discovery **2016**;6:353-67
36. Fry DW, Harvey PJ, Keller PR, Elliott WL, Meade M, Trachet E*, et al.* Specific inhibition of cyclin-dependent kinase 4/6 by PD 0332991 and associated antitumor activity in human tumor xenografts. Molecular cancer therapeutics **2004**;3:1427-38
37. Beaver JA, Amiri-Kordestani L, Charlab R, Chen W, Palmby T, Tilley A*, et al.* FDA Approval: Palbociclib for the Treatment of Postmenopausal Patients with Estrogen Receptor-Positive, HER2-Negative Metastatic Breast Cancer. Clinical cancer research : an official journal of the American Association for Cancer Research **2015**;21:4760-6
38. Zainal NS, Lee BKB, Wong ZW, Chin IS, Yee PS, Gan CP*, et al.* Effects of palbociclib on oral squamous cell carcinoma and the role of PIK3CA in conferring resistance. Cancer Biol Med **2019**;16:264-75
39. Nathan CO, Amirghahari N, Rong X, Giordano T, Sibley D, Nordberg M*, et al.* Mammalian target of rapamycin inhibitors as possible adjuvant therapy for microscopic residual disease in head and neck squamous cell cancer. Cancer research **2007**;67:2160-8

40. Molinolo AA, Hewitt SM, Amornphimoltham P, Keelawat S, Rangdaeng S, Meneses Garcia A*, et al.* Dissecting the Akt/mammalian target of rapamycin signaling network: emerging results from the head and neck cancer tissue array initiative. Clin Cancer Res **2007**;13:4964-73
41. Lui VW, Hedberg ML, Li H, Vangara BS, Pendleton K, Zeng Y*, et al.* Frequent mutation of the PI3K pathway in head and neck cancer defines predictive biomarkers. Cancer Discov **2013**;3:761-9
42. Dunn LA, Fury MG, Xiao H, Baxi SS, Sherman EJ, Korte S*, et al.* A phase II study of temsirolimus added to low-dose weekly carboplatin and paclitaxel for patients with recurrent and/or metastatic (R/M) head and neck squamous cell carcinoma (HNSCC). Annals of oncology : official journal of the European Society for Medical Oncology / ESMO **2017**;28:2533-8
43. Massarelli E, Lin H, Ginsberg LE, Tran HT, Lee JJ, Canales JR*, et al.* Phase II trial of everolimus and erlotinib in patients with platinum-resistant recurrent and/or metastatic head and neck squamous cell carcinoma. Annals of oncology : official journal of the European Society for Medical Oncology **2015**;26:1476-80
44. Grünwald V, Keilholz U, Boehm A, Guntinas-Lichius O, Hennemann B, Schmoll HJ*, et al.* TEMHEAD: a single-arm multicentre phase II study of temsirolimus in platin- and cetuximab refractory recurrent and/or metastatic squamous cell carcinoma of the head and neck (SCCHN) of the German SCCHN Group (AIO). Annals of oncology : official journal of the European Society for Medical Oncology **2015**;26:561-7
45. Saba NF, Hurwitz SJ, Magliocca K, Kim S, Owonikoko TK, Harvey D*, et al.* Phase 1 and pharmacokinetic study of everolimus in combination with cetuximab and carboplatin for recurrent/metastatic squamous cell carcinoma of the head and neck. Cancer **2014**;120:3940-51
46. Wu X, Yeerna H, Goto Y, Ando T, Wu VH, Zhang X*, et al.* Metformin Inhibits Progression of Head and Neck Squamous Cell Carcinoma by Acting Directly on Carcinoma-Initiating Cells. Cancer Res **2019**;79:4360-70
47. Wood KC, Gutkind JS. Challenges and Emerging Opportunities for Targeting mTOR in Cancer. Cancer Res **2022**;82:3884-7
48. Herrera-Abreu MT, Palafox M, Asghar U, Rivas MA, Cutts RJ, Garcia-Murillas I*, et al.* Early Adaptation and Acquired Resistance to CDK4/6 Inhibition in Estrogen Receptor-Positive Breast Cancer. Cancer research **2016**;76:2301-13
49. Cai Z, Wang J, Li Y, Shi Q, Jin L, Li S*, et al.* Overexpressed Cyclin D1 and CDK4 proteins are responsible for the resistance to CDK4/6 inhibitor in breast cancer that can be reversed by PI3K/mTOR inhibitors. Sci China Life Sci **2023**;66:94-109
50. Gu Z, Shi C, Li J, Han Y, Sun B, Zhang W*, et al.* Palbociclib-based high-throughput combination drug screening identifies synergistic therapeutic options in HPV-negative head and neck squamous cell carcinoma. BMC Med **2022**;20:175

Figure Legends

Figure 1. CRISPR screening identified cell cycle pathway as synthetic lethal pathway for mTORi in HNSCC

A. Scheme for CRISPR screening. Cal27-Cas9 cells were infected with human kinome CRIPSR knockout library, targeting 763 genes consisting of 4 gRNAs for each gene, and subjected to vehicle treatment or INK128 treatment. At population doubling (PD) 20, genomic DNA was extracted from cells, and PCR and NGS were performed. **B.** The volcano plot of all sgRNA hits. **C.** Extraction sequence of sgRNA hits. The sensitizing hits and resistance driving hits were extracted with p-value < 0.01 and analyzed with KEGG pathway analysis. **D.** Selected 109 hits plot. The hits included genes related to PI3K/mTOR and cell cycle pathways. **E.** KEGG pathway analysis for sensitizing hits. KEGG pathway analysis was applied for significant 109 hits. The top 15 pathways are represented, the color intensity of the bar represents the enrichment score. **F.** Cyclin D1 (*CCND1*) mRNA expression and overall survival in TCGA-HNSC patients. Patients with high (Z-score > 0.5, n=124) and low (Z-score < 0.5, n=73) expression of each mRNA were compared by Log-rank test. **G.** CCND1 RPPA expression and overall survival in TCGA-HNSC patients. Patients with high (Z-score > 0.5, n=120) and low (Z-score < 0.5, n=120) expression of each mRNA were compared by Log-rank test.

Figure 2. Combination of INK128 and palbociclib showed strong synergism in HNSCC cells in vitro

A. Cell viability of Cal27 and HN12 that treated with siRNAs for 24 hours, after that added INK128 (30nM) and treated for another 48 hours was measured (mean ± SEM, n = 4). **B.** The effect of INK128 on Cal27 HNSCC cells. INK128 potently blocked the cell viability with growth inhibition of 50% (GI_{50}) of 42 nM for Cal27 HNSCC cells (mean ± SEM, n = 3). **C.** The effect of palbociclib on Cal27 HNSCC cells. GI_{50} for palbociclib was 0.89 μM for Cal27 cells (mean ± SEM, n = 3). **D.** Analysis for synergism between INK128 and palbociclib by Chou-Talalay method for Cal27 cells. CI was below 1 for most percentage of fraction when cells were treated with 1:10 or 1:20 concentration of INK128 and palbociclib, respectively. **E.** Factorial dose matrix for INK128 and palbociclib. **F.** Analysis for synergism between INK128 and palbociclib by Bliss model. Strong synergism was observed with relatively higher INK128 concentration than GI_{50}. **G.** Colony formation abilities of Cal27 treated with INK128 (20nM) and/or palbociclib (0.4μM) were measured. Representative stained colony image of each treatment group. Colony area of each treatment group was compared relative to controls (mean ± SEM, n = 3). **H.** Orosphere formation abilities of Cal27 treated with INK128 (20nM) and/or palbociclib (0.4μM) were measured. Representative sphere image of each treatment group. Orosphere volume of each treatment group was compared (mean ± SEM, n = 9). ****P < 0.0001, ***P < 0.001, **P < 0.01, *P < 0.05, ns = non-significant. p-value was determined by one-way ANOVA with Tukey's post hoc test in Figure 2G and 2H. p-value was determined by two-way ANOVA with Tukey's post hoc test in Figure 2A.

Figure 3. Upregulation of CCNE1 by palbociclib confers resistance to palbociclib, which can be reverted by INK128

A. Relative mRNA levels of *CCND1* and *CCNE1* in Cal27 treated with INK128 and/or palbociclib for 24 hours. **B.** Signaling change with INK128 and/or palbociclib treatment. Cal27 was treated with 50 nM of INK128, 1μM of palbociclib, or both for 48 hours after serum starvation overnight, and were analyzed for indicated proteins by western blotting. **C.** Cell viability of Cal27 cells treated with palbociclib. Comparison of wild type, overexpressing CCND1, CCNE1 and both

(mean ± SEM, n = 3). **D.** Cell viability of Cal27 cells treated with palbociclib. Comparison of wild type, overexpressing CCNE1, CCNE1+INK128 treatment (mean ± SEM, n = 3). **E.** eIF4G binding assay with INK128 and/or palbociclib treatment for *CCNE1*. Proteins from each treated Cal27 were immunoprecipitated by eIF4G. RNA was extracted from the IP product and expression of CCNE1 was determined by qPCR (mean ± SEM, n = 3). **F.** eIF4G binding assay with INK128 and/or palbociclib treatment for *CCND1*. Proteins from each treated Cal27 were immunoprecipitated by eIF4G. RNA was extracted from the IP product and expression of CCND1 was determined by qPCR (mean ± SEM, n = 3). **G.** Schema for CCND1 and CCNE1 mRNA translation. mTORC1 phosphorylates 4EBP1 and suppresses mRNA translation. ****P < 0.0001, ***P < 0.001, **P < 0.01, *P < 0.05, ns = non-significant. p-value was determined by one-way ANOVA with Tukey's post hoc test in Figure 3A. p-value was determined by two-way ANOVA with Tukey's post hoc test in Figure 3E and 3F.

Figure 4. Combination therapy with INK128 and palbociclib is effective against HNSCC xenograft

A. Tumor growth curve for Cal27 xenograft with INK128, palbociclib, and combination (mean ± SEM, n = 10). **B.** H&E staining of Cal27 xenograft tumors. **C.** BrdU staining for Cal27 xenograft tumors. The percentage of BrdU-positive cells was compared by treatment group (mean ± SEM, n = 3). **D.** Representative IHC staining images of HN12 xenografts (strongly magnified). Tumors were stained with HE, pS6, p4EBP1, CCND1 and CCNE1. ****P < 0.0001, ***P < 0.001, **P < 0.01, *P < 0.05, ns = non-significant. p-value was determined by one-way ANOVA with Tukey's post hoc test in Figure 4A and 4C.

Figure 5. Schematic representation of the mechanism for combination treatment with INK128 and palbociclib.

Schema for untreated HNSCC, on palbociclib treatment and on combination treatment. Schematic representation of the mechanism of combination treatment with INK128 and palbociclib. See Discussion for details.

Figure 1

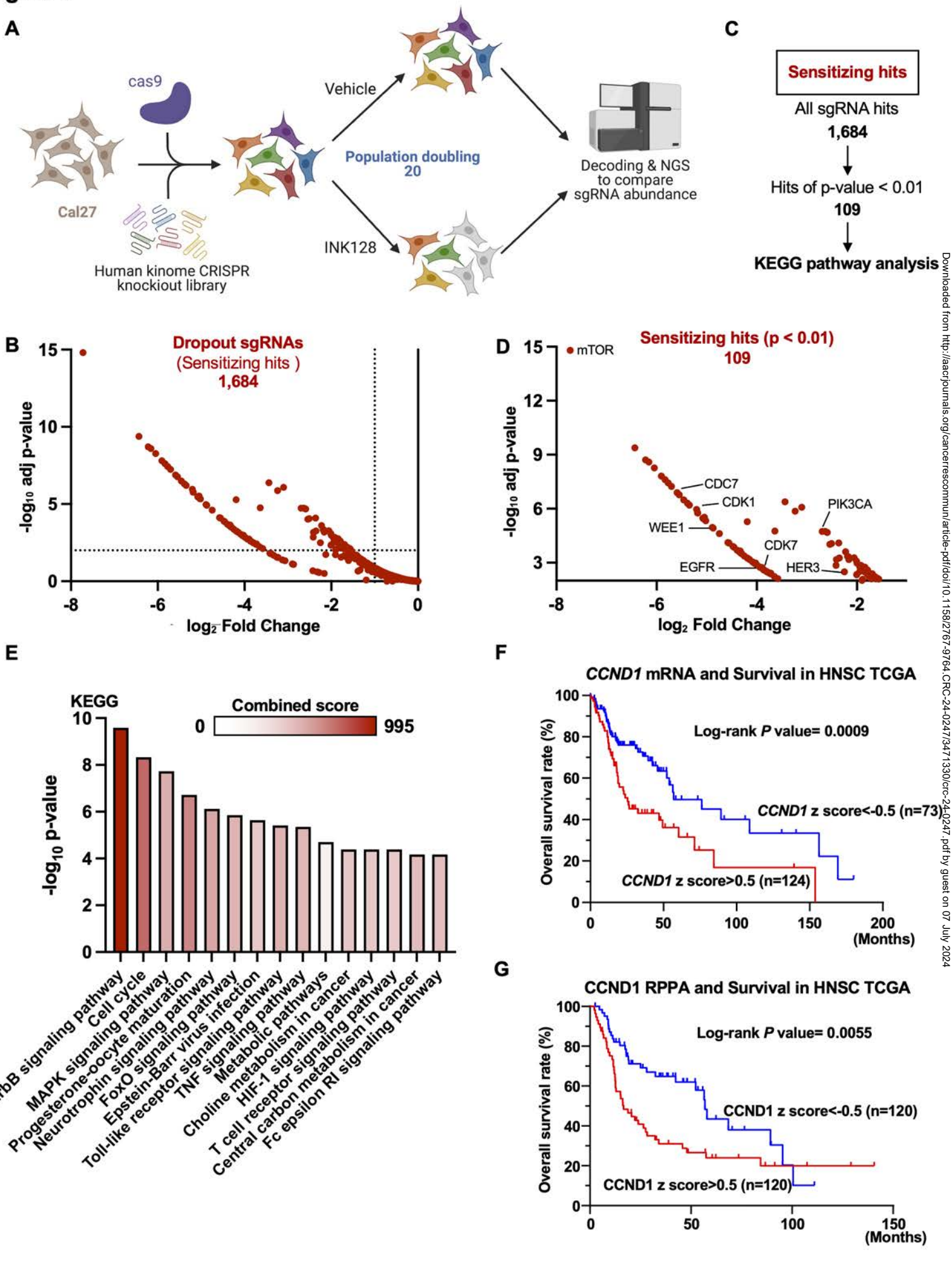

Figure 2

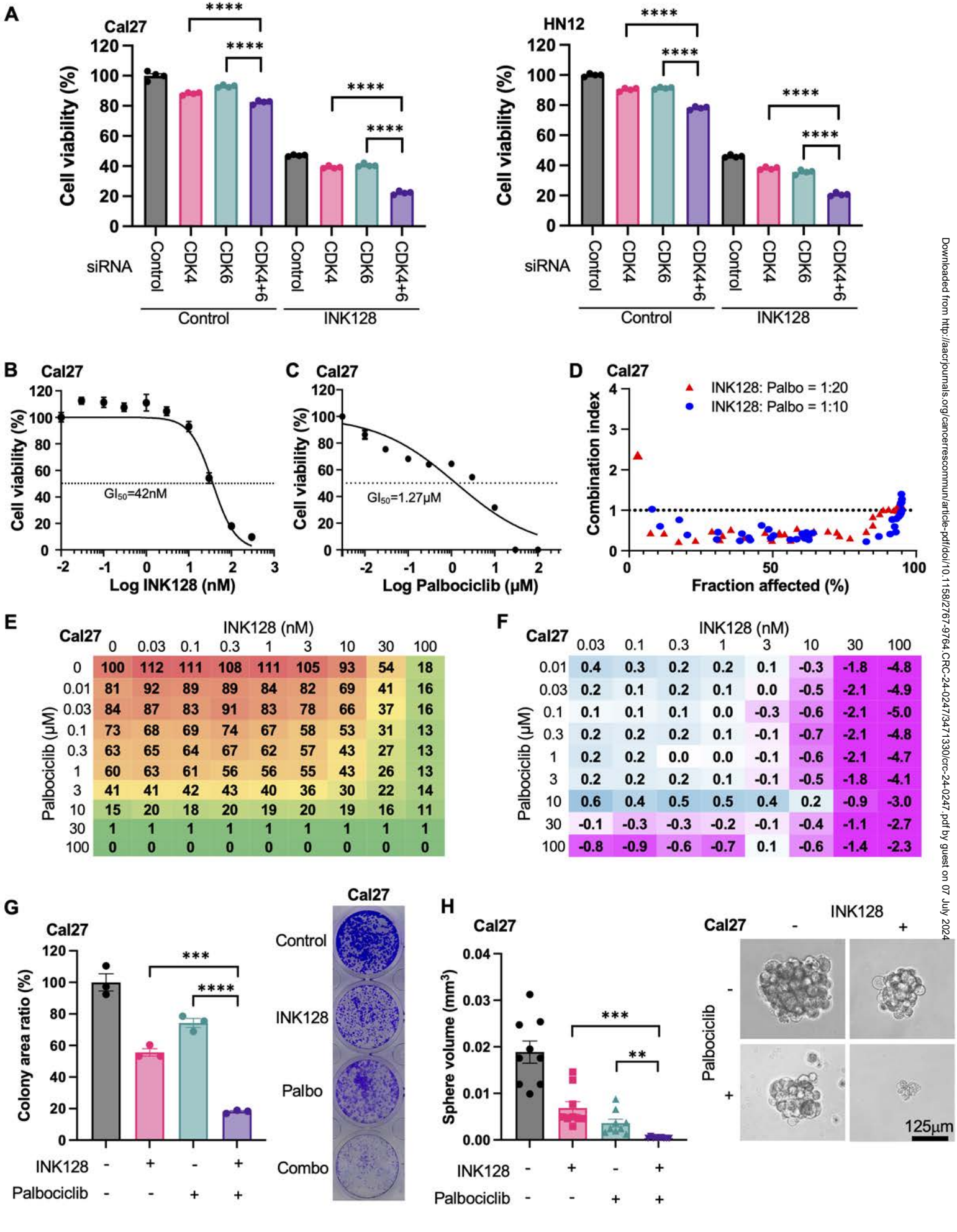

Figure 3

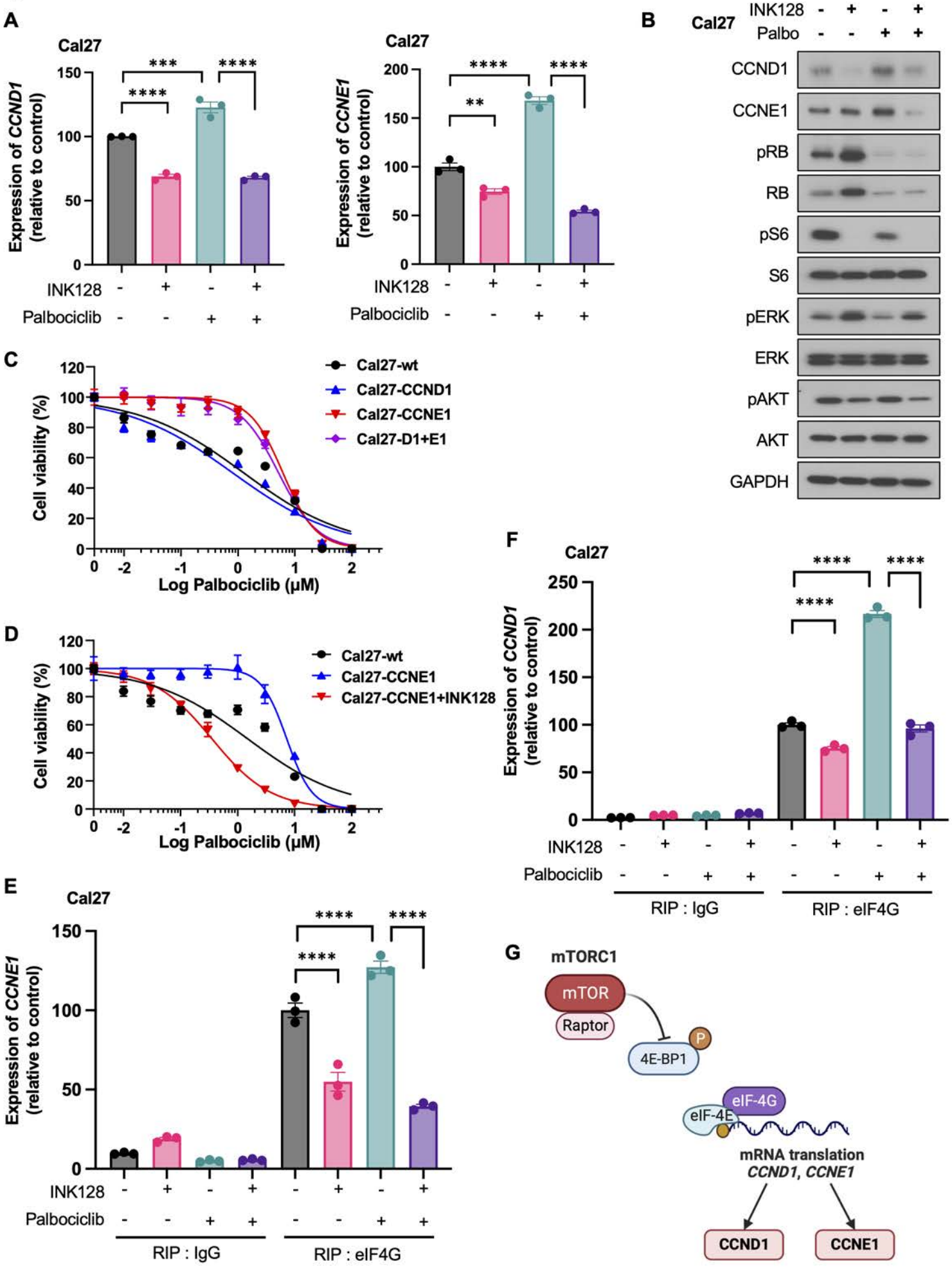

Figure 4

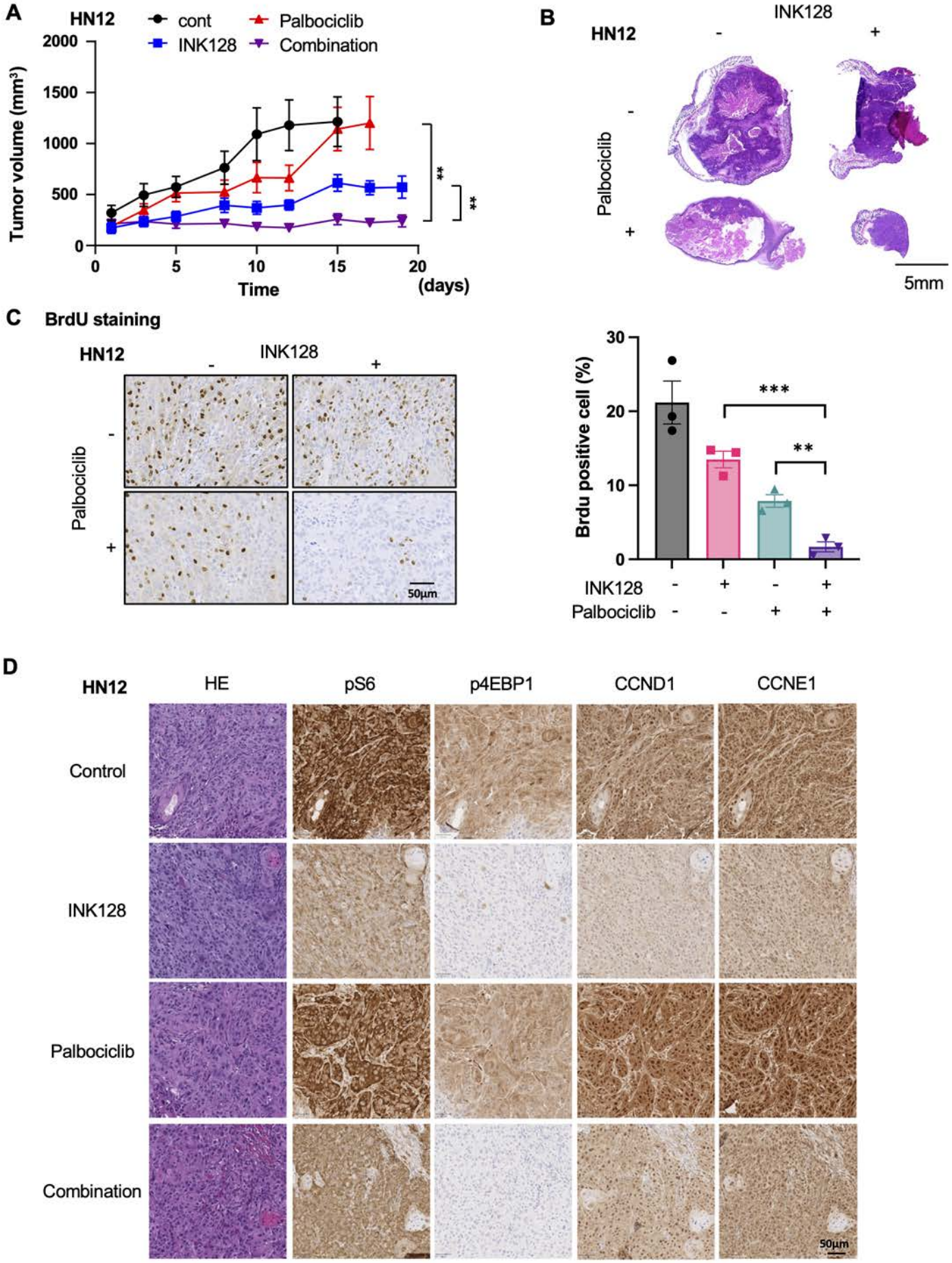

Figure 5